Available online at www.sciencedirect.com
SCIENCE DIRECT®
Journal of Photochemistry and Photobiology A: Chemistry 173 (2005) 309–318
Journal of Photochemistry and Photobiology A:Chemistry
www.elsevier.com/locate/jphotochem

Non-radiative decay in rhodamines: Role of 1:1 and 1:2 molecular complexation with β-cyclodextrin

José A.B. Ferreira *, Sílvia M.B. Costa

Centro de Química Estrutural, Instituto Superior Técnico, Av. Rovisco Pais, 1049-001 Lisboa, Portugal

Available online 31 May 2005

Abstract

The stoichiometry of complexes formed between Rhodamine 3B and Hexyl-Rhodamine B with β-cyclodextrin was investigated by electronic absorption, fluorescence spectroscopy and photokinetics and well supported by thermochromic studies. Complex 1:1 is formed at low β-cyclodextrin concentrations with Rhodamine 3B and Hexyl-Rhodamine B with estimated equilibrium constants $K_1 = 8.4 \times 10^3\,M^{-1}$ and $K'_1 = 2.1 \times 10^3\,M^{-1}$, fluorescence quantum yields $\Phi_f = 0.12$ and $\Phi'_f = 0.15$ and lifetimes $\tau_f = 610$ and $\tau'_f = 750$ ps, respectively. At higher β-cyclodextrin concentrations 1:2 (cyclodextrin) complexes are formed with estimated equilibria constants of $K_2 = 2.8\,M^{-1}$ and $K'_2 = 7.5\,M^{-1}$, fluorescence quantum yields $\Phi_f = 0.67$ and $\Phi'_f = 0.68$ and lifetimes $\tau_f = 3360$ and $\tau'_f = 3390$ ps, respectively for Rhodamine 3B and Hexyl-Rhodamine B.

The radiationless rate constants in both 1:1 complexes with either rhodamine reflect essentially the activated charge transfers which are enhanced to $k_A = (1.1–1.4) \times 10^9\,s^{-1}$ as compared to 1:2 complexes of $k_A = (7.5–7.8) \times 10^7\,s^{-1}$. The difference in one order of magnitude is assigned to the specificity of the binding sites and geometry constraints in each case.

Keywords: Non-radiative process; Molecular complex; Rhodamine; Cyclodextrin

1. Introduction

Cyclic oligomers of *R-D*-glucose – cyclodextrins (CDs) – are well known molecules and their complexation with a wide variety of compounds has been described over the years [1–4]. Three distinct CDs are commonly available consisting of six (α-CD), seven (β-CD) or eight (γ-CD) sugar units all of which have a doughnut shaped hydrophobic cavity. The cyclodextrin molecules are similar to a torus, but they are generally represented as truncated cones. The primary hydroxyl (upper) rim of the cavity has a more reduced diameter compared with the secondary (lower) hydroxyl rim. The external hydroxyl group confers a polar character whereas the interior of the cavity is non-polar relatively to the usual external environments.

Monomolecular inclusion complexes are formed with many guest molecules in particular drugs, which can enter the cavity in whole or in part. The complexation is controlled by specific interactions, polar affinity and stereochemistry of both host and guest molecular properties. The more important aspects that confer a molecular recognition role to cyclodextrins are the physico-chemical properties provided by the hydroxyl or derivatised groups and the flexibility which originates different conformers as well as the cavity size. In some cases, the symmetry can be broken and specific-binding abilities may result from this feature. Cyclodextrin molecules are thus widely used in pharmaceutical industry and form biocompatible compounds [2,4].

Rhodamine dyes are used in many biological applications such as in staining of biological tissues, specific binding to proteins and in photodynamic therapy making use of rhodamine derivatives with enhanced triplet state formation [5,6]. Conformational changes in proteins and DNA have been followed by rhodamine transient fluorescence and triplet–triplet absorption anisotropies [5]. These features make rhodamine dyes good candidates for non-covalent host–guest complexes with cyclodextrins. Synthetic novel β-cyclodextrin compounds show interesting fluorescence

* Corresponding author. Tel.: +351 21 8419318;
fax: +351 21 8464455/8464457.
E-mail address: bracons@mail.ist.utl.pt (J.A.B. Ferreira).

1010-6030/$ – see front matter © 2005 Elsevier B.V. All rights reserved.
doi:10.1016/j.jphotochem.2005.04.010

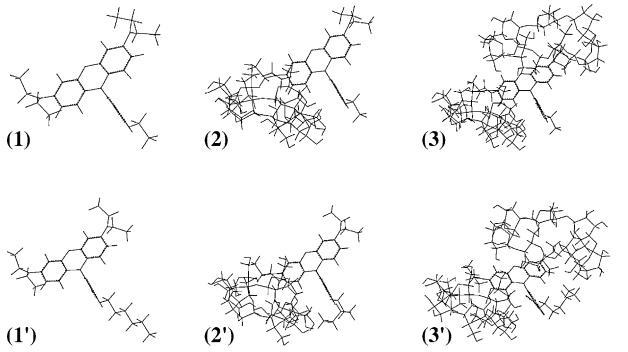

Scheme 1. Derivatives of Rhodamine B, Rhodamine 3B and Hexyl-Rhodamine B and their 1:1 and 1:2 complexes with β-cyclodextrin molecules. (**1**) Rhodamine 3B; (**2**) Rhodamine 3B:β-CD; (**3**) Rhodamine 3B:β-CD_2; (**1′**) Hexyl-Rhodamine; (**2′**) Hexyl-Rhodamine B:β-CD; (**3′**) Hexyl-Rhodamine B:β-CD_2. Molecular frameworks shown were obtained by molecular mechanics with the MM^+ force field using global geometry optimisation.

behaviour of Rhodamine B upon inclusion complexation with two cyclodextrin units [7].

In this paper, the photophysics of Rhodamine B derivatives, Rhodamine 3B (**1**) (ethyl ester of Rhodamine B) and Hexyl-Rhodamine B (**1′**) (hexyl ester of Rhodamine B) complexed with β-cyclodextrin is presented. Changes in the complexes stoichiometry are reflected in the radiationless processes, which are used as a tool to understand the effect of molecular structure and the specificity of the binding sites. We envisage that the cationic species can establish stable complexes with neutral receptors in aqueous medium. The interactions that determine the binding will be those arising from the whole charge distribution enabling that local structural effects will be reflected in the excited state behaviour. The variation of binding constants of complexes of β-cyclodextrin with rhodamine esters suggests that the ester alkyl chains have an effect in the complexes stability (Scheme 1).

2. Materials and methods

Rhodamine 3B (9′-(2-ethoxycarbonyl)-phenyl-3′,6′-bis-(diethylamino)-xanthylium, (**1**)) perchlorate (Radiant Dyes Chemie, Laser grade), Hexyl-Rhodamine B (9′-(2-hexoxycarbonyl)-phenyl-3′,6′-(diethylamino)-xanthylium, (**1′**)) chloride from Molecular Probes Inc. and β-cyclodextrin from Fluka 99% were used as received. Water was distilled twice over quartz. In all cases, the purity was checked by the absorption and fluorescence spectra in the UV/Vis range.

The samples (5 ml) were obtained using aliquots from ethanol stock solutions of the dyes evaporated with a nitrogen stream. Rhodamine 3B and Hexyl-Rhodamine B concentration was kept below 5 μM (to avoid dye aggregation and inner filter effects) by addition of increasing amounts of β-cyclodextrin solution in phosphate buffer at pH = 6. The range of experimental concentrations of β-cyclodextrin was 0–20 mM. Fresh samples were used in all the measurements. Absorption spectra were recorded with a Jasco V-560 UV/Vis spectrophotometer with blank correction. Temperature was varied in the range 280–330 K and the spectral alterations produced were recorded for Rhodamine 3B electronic absorption at different β-cyclodextrin concentrations. Fluorescence spectra were obtained at $T = 296$ K in a Perkin-Elmer LS-50B spectrofluorometer and were corrected with the curve provided with the instrument. Excitation wavelengths ($S_1 \leftarrow S_0$), were $\lambda_{exc} = 522$ nm for Rhodamine 3B and $\lambda_{exc} = 524$ nm for Hexyl-Rhodamine B. Temperature was controlled within ±1 K circulating water stream on the apparatus cell holders [8]. Fluorescence quantum yields were determined using the reference method with Rhodamine 3B in water ($\Phi_f = 0.28$) as standard previously determined against Rhodamine 6G in ethanol [9,10]. Fluorescence decays were obtained using the time-correlated single photon counting technique [12] with a Picoquant Microtime 200 fluorescence lifetime microscope (Olympus IX 71), with excitation source from a diode laser (LDH 400) promoting the rhodamine $S_2 \leftarrow S_0$ transition [11]. The back-scattered light from the 10 mm quartz rectangular cell bottom was used to obtain the instrumental response function (IRF) with FWHM = 300 ps. The time resolution of photon counting apparatus allows that a single exponential decay with a 100 ps time constant be determined. The fluorescence was collected with a long pass filter (XF30086, 510ALP) from Omega Optical, with a photomultiplier (PMA-182). The decays were analysed by iterative reconvolution of a sum of three exponential functions with the instrumental response function (IRF) using a least squares optimisation procedure with the Levenberg–Marquardt algorithm [13,14]. The quality of the fits was judged based on χ^2 values in the range 0.9–1.2 and Durbin–Watson parameters around 2 as well by inspection of weighted residuals and their autocorrelation functions.

3. Results

3.1.1. Steady state absorption and emission electronic spectroscopy

The effect of the complexation of Rhodamine 3B and Hexyl-Rhodamine B is exhibited on the absorption spectra [15–18] of rhodamines by an increase in the intensity of the 1–0 vibronic and also by a small red shift in the 0–0 transition of the chromophoric aminoxanthylium part [19,20]. This is used to monitor structural differences between the complexes with two molecules that only differ in the alkyl chain size in the carboxyphenyl group. In the range of β-cyclodextrin concentration 0–200 μm, while Rhodamine 3B spectra show an increase in 1–0 vibronic intensity without a shift in the 0–0 maximum of absorption, Hexyl-Rhodamine B spectra shows also a red shifted maximum of absorption accompanying the 1–0 vibronic increase. In this case, a crossing point is also

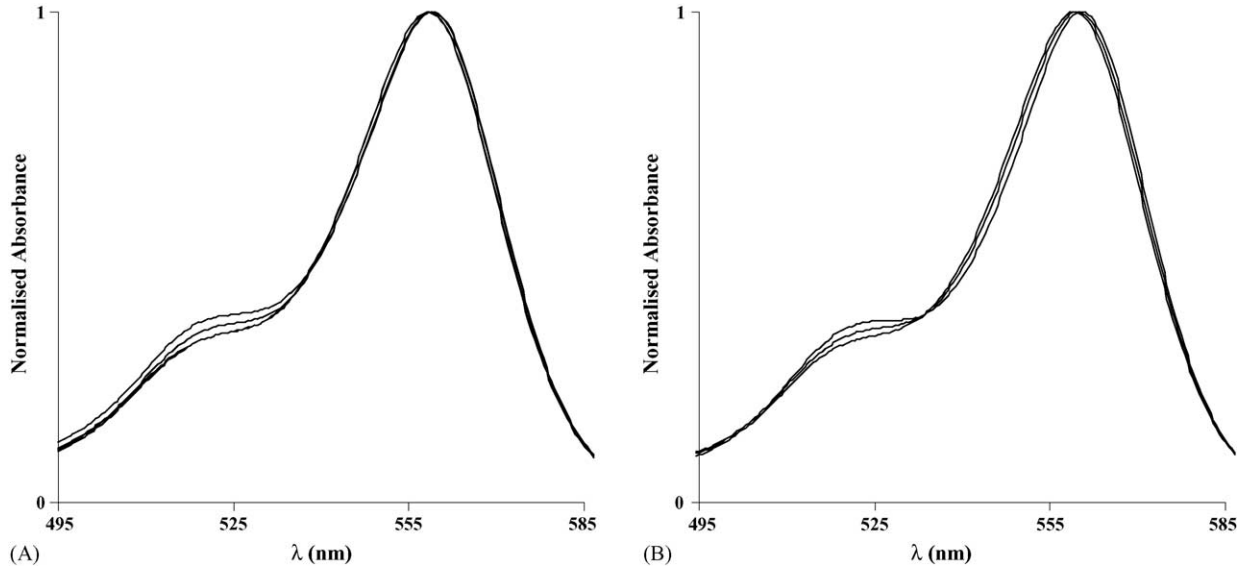

Fig. 1. Absorption spectra of ester derivatives of Rhodamine B in water at pH = 6 with increasing β-cyclodextrin concentration. (A) Rhodamine 3B, [β-cyclodextrin] = 1 μM, [β-cyclodextrin] = 87 μM, [β-cyclodextrin] = 160 μM. (B) Hexyl-Rhodamine B, [β-cyclodextrin] = 0 μM, [β-cyclodextrin] = 20 μM, [β-cyclodextrin] = 100 μM.

detected which is not observed in the Rhodamine 3B spectra at similar concentrations of β-cyclodextrin (Fig. 1). The thermochromic variations [15–18,21] also show characteristics of the presence of different species in solution (Fig. 2). The variation of the logarithmic absorbance with the temperature in the concentration region where the 1:1 complex is the prevalent species has a slope smaller than the free cationic species' in water. On the other hand, in the 1:2 complex region the slope is greater than the latter (Fig. 3).

3.2. Fluorescence quantum yields

The fluorescence quantum yields of buffered water solutions of Rhodamine 3B changes abruptly with the concentration of β-cyclodextrin around 1 mM and increases slightly in the following decade till 10 mM. A similar decrease of the higher fluorescence quantum yields of Hexyl-Rhodamine B is observed in the comparable concentration region of β-cyclodextrin and then rises clearly at higher concentrations (Fig. 4).

3.3. Transient fluorescence spectroscopy

The transient fluorescence decay profiles of Rhodamine 3B and Hexyl-Rhodamine B also show clear differences (Fig. 5). While for Rhodamine 3B a short component (around 600 ps) appears as the dominant feature in the fluorescence decays at the lower β-cyclodextrin concentrations, in Hexyl-Rhodamine B the contribution of the short component is smaller. Furthermore while in Rhodamine 3B a long lived component (around 3300 ps) appears only at the higher β-cyclodextrin concentrations, the corresponding component is readily noticed in Hexyl-Rhodamine B already at low β-cyclodextrin concentrations. In both cases, the typical lifetime of the free fluorophore in water (around 1450 ps) is detected in all decays, but as β-cyclodextrin is added, the weight decreases, giving rise to the other two components in both cases.

4. Theory and calculation

The present results are interpreted considering that two non-covalent complexes are formed between Rhodamine B and Hexyl-Rhodamine B and β-cyclodextrin molecules (Scheme 2). Primes (′) denoting data for Hexyl-Rhodamine B are omitted in general results.

4.1. Ground state equilibrium

In the ground electronic state the following mass balance can be applied to the species *X*, *Y* and *Z*, respectively the free cationic rhodamine, the 1:1 complex of *X* with β-cyclodextrin and the 1:2 complex of *X* with β-cyclodextrin:

$$C = [X] + [Y] + [Z] \quad (1)$$

$$C_{\beta\text{-cd}} = [Y] + [Z] + [\beta\text{-CD}] \quad (2)$$

$$K_1 = \frac{[Y]}{[X][\beta\text{-CD}]} \quad (3)$$

$$K_2 = \frac{[Z]}{[Y][\beta\text{-CD}]} \quad (4)$$

The capital C and $C_{\beta\text{-cd}}$ refer to the total rhodamine and β-cyclodextrin molar concentrations in solution, respectively, and the other symbols have the usual meaning. In the

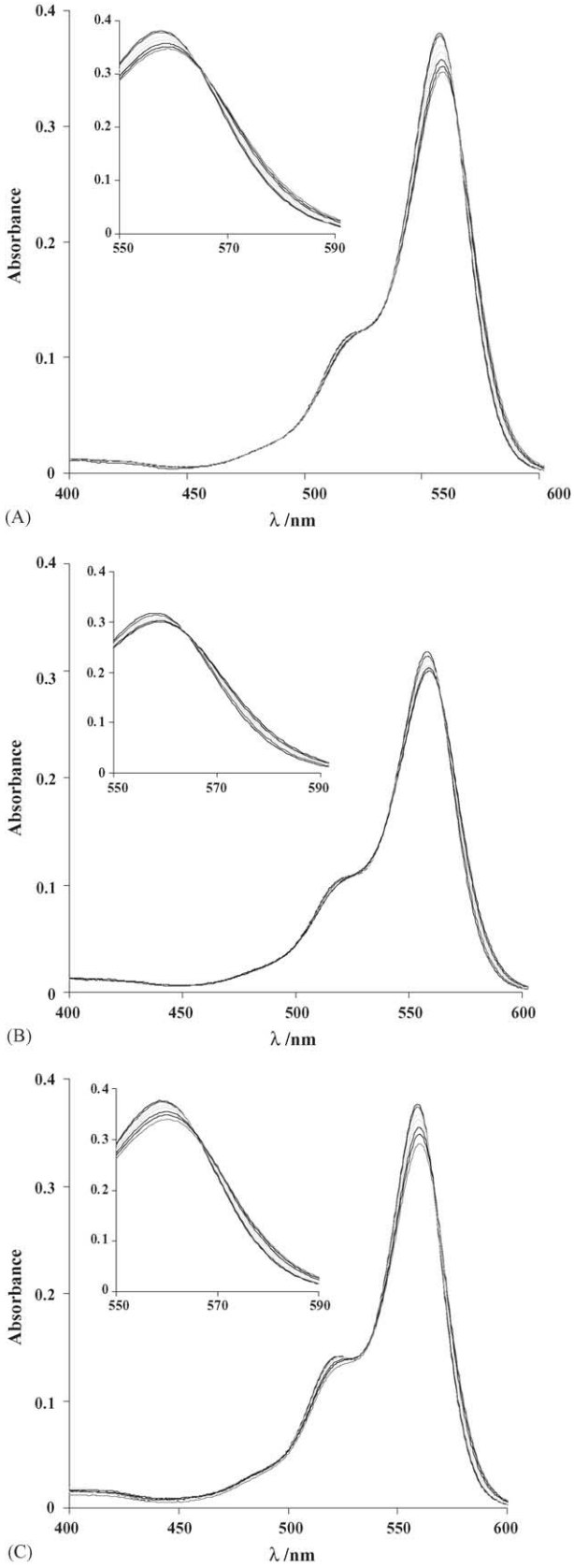

Fig. 2. Rhodamine 3B absorption ($S_2 \leftarrow S_0$; $S_1 \leftarrow S_0$) thermochromic variations (T: 281, 284, 293, 302, 311, 321, 330 K) at pH = 6 in water (A); [β-cyclodextrin] = 30 μM (B) and [β-cyclodextrin] = 6 mM (C).

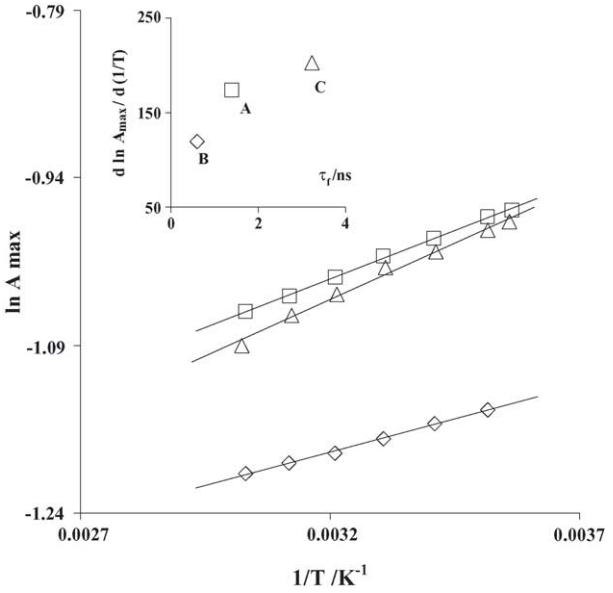

Fig. 3. Rhodamine 3B logarithmic absorbance, A_{max}, at absorption maximum ($S_1 \leftarrow S_0$) as function of the reciprocal temperature in: water (A), [β-cyclodextrin] = 30 μM (B) and [β-cyclodextrin] = 6 mM (C), (A (□); B (◇); C (△)). Inset: Representation of the slopes, $d \ln A_{max}/d\,(1/T)$, as function of the fluorescence lifetime, τ_f (ns), of the dominant species in each β-concentration region (X, Y, Z).

conditions used in the present work $C_{\beta\text{-cd}} \gg C$ in all solutions of β-cyclodextrin|rhodamine in pH 6 buffered water.

4.2. Fluorescence quantum yields variation

The total fluorescence quantum yield, Φ_f can be calculated using Eq. (5). Equal extinction coefficients at the excitation

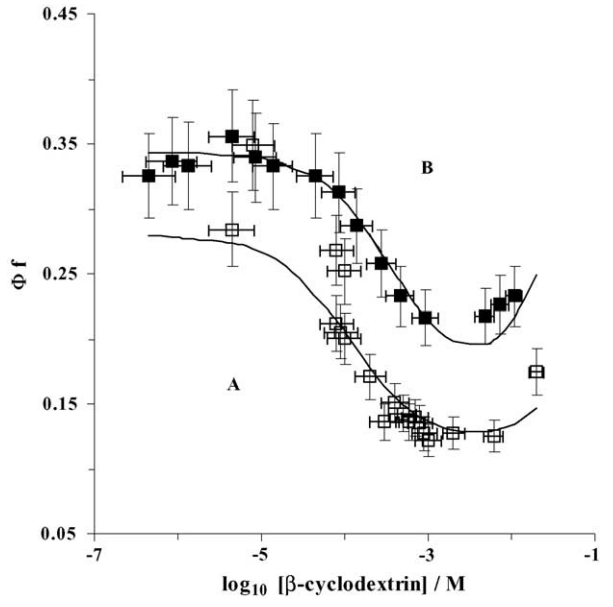

Fig. 4. Ester Rhodamines B′ fluorescence quantum yields in water at pH = 6 as function of β-cyclodextrin concentration. (A) Rhodamine 3B; (B) Hexyl-Rhodamine B. Curves correspond to calculation using Eq. (5).

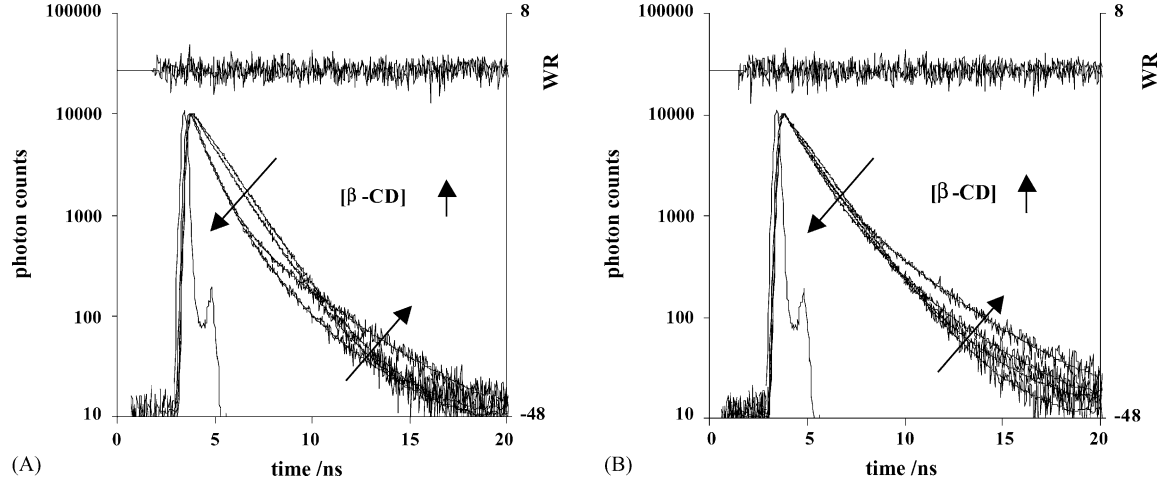

Fig. 5. Fluorescence decays of ester Rhodamines B in water at pH = 6 with different [β-cyclodextrin] = 0, 90, 900 and 9000 μM are indicated by counter-clockwise arrows from bottom to top. (A) Rhodamine 3B; (B) Hexyl-Rhodamine B. The instrumental response function, as well as typical weighed residuals are included.

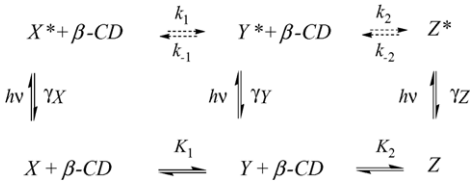

Scheme 2. Kinetic scheme proposed for ground and excited state interaction of ester derivatives of Rhodamine B with and β-cyclodextrin molecules in electronic ground and excited singlet-states.

wavelength and the ground state equilibrium are considered for the calculation of the fractions of light absorbed by each species

$$\Phi_f = \frac{\Phi_X + \Phi_Y K_1 C_{\beta\text{-cd}} + \Phi_Z K_1 K_2 C^2_{\beta\text{-cd}}}{1 + K_1 C_{\beta\text{-cd}} + K_1 K_2 C^2_{\beta\text{-cd}}} \quad (5)$$

The equilibria constants and individual fluorescence quantum yields used can be obtained from the analysis of the fluorescence decays described in the next section.

4.3. Fluorescence decay kinetics

The analysis of the fluorescence decays yields a set of decay rate constants and pre-exponential factors. The reciprocal decay rate constants are represented in Fig. 6.

The experimental decay rate constants are invariant with the β-cyclodextrin concentration. Thus, to a first approximation, it is possible to postulate that the dominant rate processes are the natural species decays to the ground sate. In these conditions, from the system of differential equations extracted from Scheme 2, it is possible to derive expressions for the normalised pre-exponential factors and evaluate the yielded description of the experimental data.

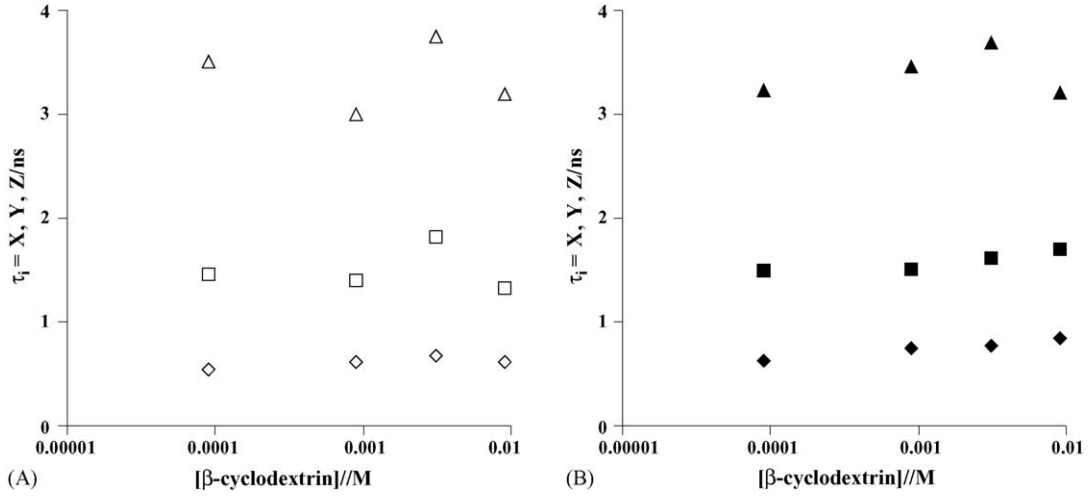

Fig. 6. Decay constants obtained from the iterative reconvolution of instrumental response function (IRF) with a sum of three exponential functions and the experimental fluorescence decays in water at pH = 6 with varying β-cyclodextrin concentration. (A) Rhodamine 3B: τ_X (□); τ_Y (◇); τ_Z (△). (B) Hexyl-Rhodamine B: τ'_X (■); τ'_Y (◆); τ'_Z (▲).

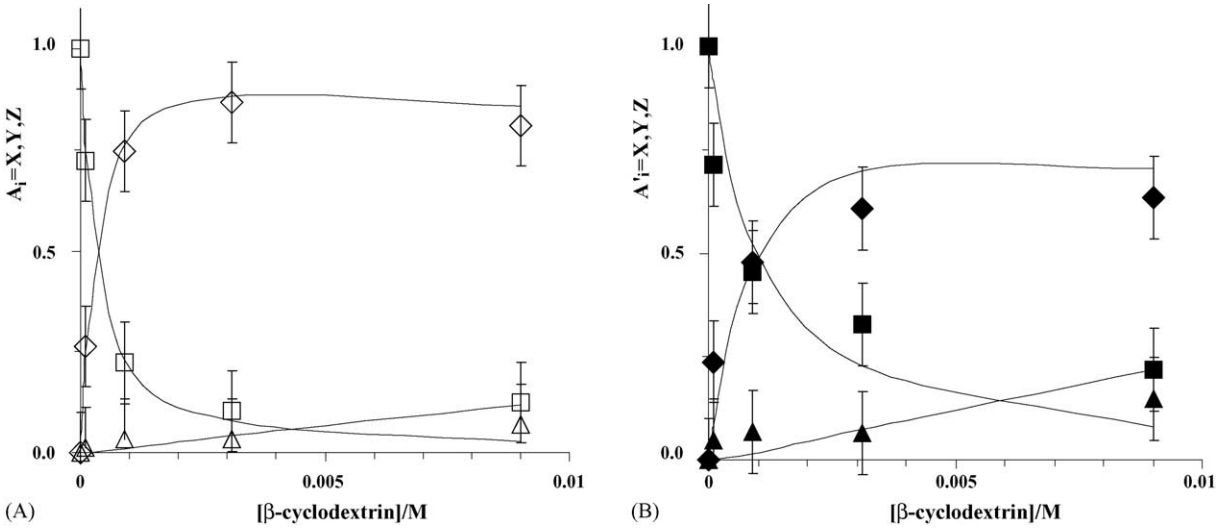

Fig. 7. Ester Rhodamines B and their β-cyclodextrin complexes' pre-exponential factors obtained from fluorescence decays in water at pH = 6 with varying β-cyclodextrin concentration. (A) Rhodamine 3B: A_X (□); A_Y (◊); A_Z (△). (B) Hexyl-Rhodamine B: A'_X (■); A'_Y (♦); A'_Z (▲). Lines are least squares global fits using Eqs. (6)–(8).

The expressions obtained considering the excited population obtained at time zero and the decay, with inclusion of the mass balance, Eqs. (1)–(4), are as follows (where the asterisk denoting excited species not included for a simpler notation):

$$A_X = \frac{1}{1 + \frac{\Phi_Y}{\Phi_X} K_1 C_{\beta\text{-cd}} + \frac{\Phi_Z}{\Phi_X} K_1 K_2 C^2_{\beta\text{-cd}}} \quad (6)$$

$$A_Y = \frac{1}{\frac{\Phi_X}{\Phi_Y} \frac{1}{K_1 C_{\beta\text{-cd}}} + 1 + \frac{\Phi_Z}{\Phi_Y} K_2 C_{\beta\text{-cd}}} \quad (7)$$

$$A_Z = \frac{1}{\frac{\Phi_X}{\Phi_Z} \frac{1}{K_1 K_2 C^2_{\beta\text{-cd}}} + \frac{\Phi_Y}{\Phi_Z} \frac{1}{K_2 C_{\beta\text{-cd}}} + 1} \quad (8)$$

Calculated fluorescence quantum yields using the fluorescence decay time constants and known k_f values ($k_f = 2 \times 10^8\ s^{-1}$ [10]) are $\Phi_X = 0.28$, $\Phi_Y = 0.12$ and $\Phi_Z = 0.67$ for Rhodamine 3B and $\Phi'_X = 0.32$, $\Phi'_Y = 0.15$ and $\Phi'_Z = 0.68$ for Hexyl-Rhodamine B. The quantum yields for individual species (**1**) and (**1′**) as well as for the corresponding species' complexes are similar although a slight increase occurs for Hexyl-Rhodamine B. Calculated values reproduce well the experimental fluorescence quantum yield data (Fig. 4).

Using Eqs. (6)–(8), the experimental pre-exponential factors are calculated. Each species' fluorescence quantum yields are used and the equilibrium constants for the range of experimental concentrations of β-cyclodextrin are estimated. The result of the global fit of Eqs. (6)–(8) to the experimental data sets of fluorescence decays pre-exponential factors obtained for Rhodamine 3B and Hexyl-Rhodamine B in the presence of various concentrations of β-cyclodextrin is shown in Fig. 7. Data is given in Table 1.

The estimated equilibria constants for Rhodamine 3B ($K_1 = 8.4 \times 10^3\ M^{-1}$ and $K_2 = 2.8\ M^{-1}$) and for Hexyl-Rhodamine B ($K'_1 = 2.1 \times 10^3\ M^{-1}$ and $K'_2 = 7.5\ M^{-1}$) show that the 1:1 complex is more extensively formed than the 1:2 complex. The data estimated herein is compatible with literature data obtained for complexes of Rhodamine B with substituted cyclodextrins [7] and for complexes of Pyronine B and Pyronine Y with β-cyclodextrin [22].

Furthermore, the analysis shows clear differences between the results obtained in each case. One can see that the approximate description undertaken gives a result consistent with all the approximations made so far. For Rhodamine 3B, the formation constant K_1 is higher than K'_1 for Hexyl-Rhodamine B possibly due to stereochemical hindrances imposed in aqueous media by the hexyl group in the binding to β-cyclodextrin in a 1:1 asymmetric structure. Moreover, one can ascertain, that the formation constant K'_2 is higher for Hexyl-Rhodamine B. In fact, although both 1:2 complexes of β-cyclodextrin with either Rhodamine 3B or Hexyl-Rhodamine B present structures less asymmetric than the 1:1 complexes', the length of the hexyl group relatively to the ethyl group should compensate the entropy loss upon weaker aqueous solvation and favour the binding, since a higher number of conformations are possible in the Hexyl-Rhodamine B:β-cyclodextrin 1:2 complex.

Host–guest dynamics should affect the excited state kinetics. However, their contribution will be small in the time scale of observation (100 ps) obtained from the calculation of Eq. (A.1) supporting the experimental results (Appendix A). Moreover, the contribution from solvation dynamics arising from the dipole moment variation upon Rhodamine 3B excitation ($\Delta\mu = 1.7D$ [20]) contrasts with higher dipole moment variations involved in the relaxation of water molecules in Coumarin 480:γ-CD complex [3,23].

Table 1
Ester Rhodamines B and their β-cyclodextrin complexes' fluorescence lifetimes and pre-exponential factors obtained from experimental fluorescence decays. Pre-exponential factors calculated using Eqs. (6)–(8) are also included

[β-CD] (μM)	(1)			(2)			(3)			(1′)			(2′)			(3′)		
	τ_X (ns)	A_X	A_X, Eq. (6)	τ_Y (ns)	A_Y	A_Y, Eq. (7)	τ_Z (ns)	A_Z	A_Z, Eq. (8)	τ'_X (ns)	A'_X	A'_X, Eq. (6)	τ'_Y (ns)	A'_Y	A'_Y, Eq. (7)	τ'_Z (ns)	A'_Z	A'_Z, Eq. (8)
0	1.437	1.000	–	–	–	–	–	–	–	1.489	1.000		–	–	–	–	–	–
90	1.456	0.723	0.751	0.538	0.264	0.249	3.512	0.013	0.000	1.490	0.714	0.918	0.630	0.237	0.082	3.230	0.048	0.000
900	1.401	0.222	0.229	0.616	0.746	0.760	2.994	0.032	0.010	1.509	0.455	0.522	0.743	0.478	0.464	3.458	0.067	0.014
3100	1.823	0.102	0.077	0.680	0.866	0.881	3.743	0.032	0.041	1.615	0.328	0.228	0.769	0.607	0.698	3.689	0.066	0.074
9000	1.331	0.123	0.026	0.615	0.809	0.857	3.195	0.068	0.117	1.700	0.218	0.079	0.846	0.635	0.704	3.200	0.147	0.217

4.4. Non-radiative rate constants

The radiationless process in both rhodamines is similar since it is known to be determined by the diethyl amino group substitution that is the same in both molecules [10,24]. From the assumptions made earlier for the Rhodamines' complexes with β-cyclodextrin, the decay constants enable the intrinsic fluorescence lifetimes of each species to be determined as given in general by Eq. (9), where the subscripts (*X*, *Y* and *Z*) have been withdrawn for the sake of a simpler notation

$$\tau_f^{-1} = k_f + k_{nr} \tag{9}$$

The radiative rate constant, k_f, is only affected by the refractive index – the Strickler–Berg equation [25] – and since very small variations in extinction coefficients occur with the increase of β-cyclodextrin concentration the approximation $k_{f,Y} = k_{f,Z} = k_f$ is acceptable [10]. Moreover, only a small effect on the extinction coefficients on complexation of Pyronines with CDs was reported [22].

The contributions to the non-radiative decay can be calculated from Eq. (10)

$$k_{nr} = k_{ic} + k_A + k_{isc} \tag{10}$$

The contribution of k_{isc} [26] to k_{nr} can be neglected since it is two orders of magnitude smaller than k_{ic} ($2 \times 10^7\ s^{-1}$) previously determined [24]. Thus, the activated non-radiative decay k_A ($\gg 10^7\ s^{-1}$) is the dominant contribution to the radiationless decay in either the free cationic species in water or in the molecular complexes with β-cyclodextrin.

4.5. Application of background knowledge about k_A

The photophysical parameters determined in representative solvents for Hexyl-Rhodamine B are similar to those of Rhodamine 3B and the differences in k_A will be indicative of variations in the excited potential energy surfaces in both 1:1 and 1:2 complexes with β-cyclodextrin. In fact, the fluorescence lifetimes in water suggest that for Hexyl-Rhodamine B, the nature of the activated radiationless process may not be significantly altered by the presence of the hexyl group. For the 1:1 complex of Rhodamine 3B with one β-cyclodextrin a fluorescence lifetime $\tau_{f,Y} = 610$ ps corresponds to an activated radiationless rate constant $k_{A,Y} = 1.4 \times 10^9\ s^{-1}$ while for 1:2 complex of Rhodamine 3B with β-cyclodextrins a fluorescence lifetime $\tau_{f,Z} = 3.36$ ns yields $k_{A,Z} = 7.8 \times 10^7\ s^{-1}$. For Hexyl-Rhodamine B $\tau_{f,Y} = 750$ ps yields $k_{A,Y'} = 1.1 \times 10^9\ s^{-1}$ while for the 1:2 complex of Hexyl-Rhodamine B with β-cyclodextrin from the fluorescence lifetime $\tau'_{f,Z'} = 3.39$ ns, $k_{A,Z'} = 7.5 \times 10^7\ s^{-1}$ is determined.

The interpretation of the activated radiationless decay in Rhodamine 3B presented earlier [10,24] relied on Grote–Hynes theory [27]. Therein, we have attempted to quantify the polarity and friction effects on the rate constant k_A in a wide variety of solvents spanning different polarities

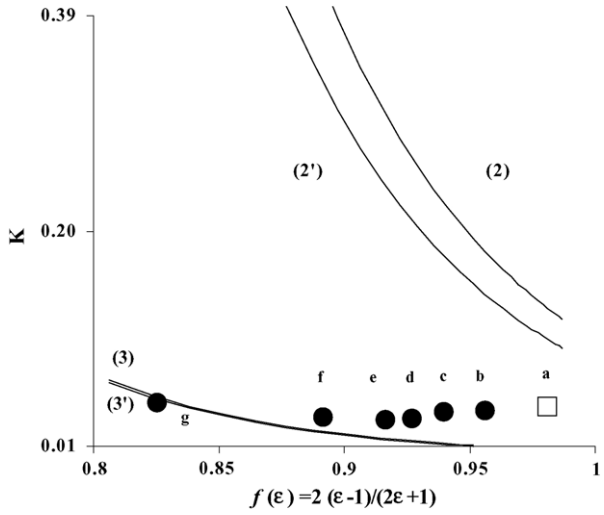

Fig. 8. Transmission coefficients obtained from the radiationless decay rate constants, Eq. (11) as function of total dielectric polarisation for ester Rhodamines B and their β-cyclodextrin complexes – 1:1 complexes: upper curves; 1:2 complexes: bottom curves. Transmission coefficients for Rhodamine 3B in various solvents [10] are shown superimposed to the complexes' data. Water (a), methanol (b), ethanol (c), 1-propanol (d), 1-butanol (e), 1-hexanol (f) and 1-decanol (g).

and viscosities. These effects could be identified using Eq. (11)

$$k_A = \kappa_{GH} \frac{\omega_0}{2\pi} e^{-E_0/k_B T} \quad (11)$$

where ω_0 is the angular frequency which characterises the activated radiationless process reactant well, κ_{GH}, the transmission coefficient of the reaction reflects friction effects on the rate constants while static polarity effects enter the rate through E_0, the height of the potential barrier relative to the bottom of the well. The reaction wavenumber, $\omega_0/2\pi c = 30\ cm^{-1}$ previously obtained as well as the dependence on the total dielectric polarisation E_0 (kJ mol^{-1}) = 31–42$f(\varepsilon)$ [10] are used in Eq. (11) to extract κ [$f(\varepsilon)$]. Herein, we attempt to estimate κ for the 1:1 and 1:2 complexes using the activated rate constants given above.

The estimated $\kappa[f(\varepsilon)]$ for the transmission coefficients, κ, as functions of the (unknown) local dielectric constant, ε, are shown in Fig. 8 together with representative results obtained with Rhodamine 3B in solvents. The representations suggest that the dynamic effects contained in the transmission coefficients as well as the local polarity sensed by the reaction co-ordinates upon complexation are quite different for both rhodamines' 1:1 complexes with β-cyclodextrin. The dynamic situation felt at the interaction sites of Rhodamine 3B and Hexyl-Rhodamine B 1:1 and 1:2 complexes with β-cyclodextrin is reflected by transmission coefficients estimated. While the $\kappa[f(\varepsilon)]$ obtained for the 1:2 complexes is essentially the same for the two rhodamine molecules and falls within the 1-decanol's and 1-hexanol's transmission coefficients, the same does not happen with the $\kappa[f(\varepsilon)]$ of the 1:1 complexes. In fact, the estimated transmission coefficients, κ, for the 1:1 complexes are higher than the highest previously found in water at the same temperature [10].

Rhodamine 3B fluorescence lifetimes close to those experimentally observed herein could be nearly reproduced using Grote–Hynes theory with viscoelastic modelling of the dynamic friction ([10] and references cited therein). For instance, in ethanol at $T = 341$ K ($\varepsilon_r = 18$ and $\eta_s = 0.5$ cP), $\tau_f = 610$ ps. In 1-decanol at $T = 293$ K ($\varepsilon_r = 8$ and $\eta_s = 12$ cP) $\tau_f = 3.26$ ns and in 1,3-propanediol ($\varepsilon_r = 35$ and $\eta_s = 40$ cP), $\tau_f = 3.25$ ns. Similarities can easily be established with 1:2 complexes' fluorescence efficiency. However, considering the former case comparatively to that of the 1:1 complexes, the correlations obtained (Fig. 8) imply that another driving force is present. The increased efficiency in the radiationless process may be associated to possible causes that act synergistically, which will be advanced in Section 5.

5. Discussion

The description made based on the radiationless decay rate constant is consistent with the spectral variations observed in the formation of both types of complexes. In the case of 1:1 complex one finds an increase in the 1–0 vibronic with no red shift in the 0–0 vibronic band of maximum absorption. The increased vibronic weight can be related to the population of higher frequency modes, consistent with the occurrence of geometry constraints upon complexation. Oppositely, in the 1:2 complex one also finds a red shift in absorption maximum [20,21] spanned by the 0–0 vibronic upon the increase of β-cyclodextrin concentration. This can be interpreted as arising from an average lower polarity environment felt by the aminoxanthylium chromophore. At the maximum of Gaussian sub-bands, the extinction coefficient in linked with the bandwidth [21]. A larger width is predicted for higher solvent polarisation and is related to enhanced mode coupling. Consequently, shorter state lifetimes are expected. A clear correlation can be seen between the slope of the temperature variation of the logarithmic maximum absorption [20] and the fluorescence lifetime, τ_f, of the dominant species in each characteristic β-cyclodextrin concentration region (inset of Fig. 3). Furthermore, the extinction coefficient at the maximum decreases with increasing temperature but increases at lower wavelengths in line with enhanced participation of lower frequency intermolecular energy dissipating modes (inset of Fig. 2).

The ground state equilibrium constant for the formation of 1:1 complex of Rhodamine 3B with β-cyclodextrin is threefold higher than the corresponding 1:1 complex of ground state Hexyl-Rhodamine B. On the other hand, the equilibrium constant for the formation of 1:2 complexes between Rhodamine 3B and two β-cyclodextrin molecules is nearly three-fold lower than for Hexyl-Rhodamine B. We interpret the differences as due to the enhanced stereochemical hindrance induced by the hexyl group to the binding of

Hexyl-Rhodamine B to the β-cyclodextrin molecule as compared to that of the shorter ethyl chain of Rhodamine 3B.

The observed trend is also reflected in the fluorescence lifetimes whose differences arise from the radiationless rate constant, k_{nr} of the two complexed forms. In fact, while the 1:1 complex has a much shorter lifetime than the free rhodamine cationic species in water that of the 1:2 complex has a longer fluorescence lifetime.

Host–guest geometry restriction and/or dielectric coupling can affect the radiationless transitions. In the former case, a funnel can be achieved that enhances the reaction coordinate progression by increased torsion. On the other hand, increased efficiency may occur if the dipole involved in the adiabatic charge transfer event [10,24] participating in the radiationless process is oriented in such way that it can couple to the β-cyclodextrin molecular dipoles, thus enhancing the polarity dependence of the rate constant.

The polar diethyl amino groups should be good binding sites to the β-cyclodextrin (see Scheme 1) and are likely to be responsible for the observed differences in the non-radiative rate constants of 1:1 and 1:2 complexes. In the 1:1 complex the amino group of the rhodamine molecule senses an asymmetrical charge distribution provided by the interaction with one β-cyclodextrin molecule thus enhancing the activated radiationless decay rate constant. The ester alkyl chain group hinders the penetration of *N*-alkyl group in the non-polar cavity. In fact, the data shows that the 1:1 complex with Rhodamine 3B has a more efficient radiationless process as is inferred by the calculated transmission coefficients. On the other hand, the lower transmission coefficient in Hexyl-Rhodamine B suggests a clue for an explanation – a funnel for C=N rotation caused by stereochemical restrictions imposed by asymmetric docking. In the case of the 1:2 complex the more symmetrical charge effect provided by the interaction with the two β-cyclodextrin molecules, each one with a single amino group contributes to hinder the evolution in the rotational co-ordinate. In this case, the penetration depth should be less constrained since the asymmetric dipole–dipole interaction can cancel. In this situation, the nitrogen atoms of the Rhodamine molecules sense the low polarity of the β-cyclodextrin cavity and the friction effects will determine the absence of evolution in the radiationless decay reaction coordinate. At this level, the interaction with the alkyl chain of the carboxyphenyl ester group does not play any role since the β-cyclodextrin molecules are directed in orthogonally directed planes.

6. Conclusion

The interaction of two ester derivatives of Rhodamine B with β-cyclodextrin molecules was studied using steady state electronic absorption, thermochromic spectral variations, steady state and transient state fluorescence. The formation constants of 1:1 and 1:2 complexes with both Rhodamine B derivatives as well as their fluorescence quantum yields were obtained from modelling transient fluorescence and agree well with the variation of the total fluorescence quantum yields of both dyes.

Attempts to interpret the variation trend of rate constants in these complexes with structural aspects were made through correlations of the transmission coefficients with polarity functions. Significant changes in the 1:1 relatively to 1:2 complexes were assigned to the specificity of binding sites and geometry constraint in each case.

Acknowledgements

The work was supported by FCT Project POCTI/35398/99 and J.A.B.F. postdoctoral grants PRAXIS XXI/BPD/22090/99 and POCTI/SFRH/BPD/11568/2002. Mr. M. Tavares is acknowledged for performing in part the steady state measurements.

Appendix A. Determination of kinetic decay constants in the three-state-excited state (Scheme 2)

The system of linear differential equations that is derived from the excited states populations (*) and b (standing for β-cyclodextrin concentration) in Scheme 2 with instant photon absorption and time independent rate constants produces decay constants, λ_1, λ_2 and λ_3, that are obtained from the solution of Eq. (A.1)

$$\begin{vmatrix} -(\gamma_X + k_1 b) - \lambda & k_{-1} & 0 \\ k_1 b & -(\gamma_Y + k_{-1} + k_2 b) - \lambda & k_{-2} \\ 0 & k_2 b & -(\gamma_Z + k_{-2}) - \lambda \end{vmatrix} = 0 \tag{A.1}$$

Eq. (A.1) yields the cubic equation, Eq. (A.2):

$$\lambda^3 + \lambda^2\beta + \lambda\gamma + \delta = 0 \tag{A.2}$$

where

$$\beta = (\gamma_X + k_1 b) + (\gamma_Y + k_{-1} + k_2 b) + (\gamma_Z + k_{-2}) \tag{A.3}$$

$$\gamma = (\gamma_X + k_1 b)[(\gamma_Y + k_{-1} + k_2 b) + (\gamma_Z + k_{-2})] + (\gamma_Y + k_{-1} + k_2 b)(\gamma_Z + k_{-2}) - (k_{-2}k_2 + k_{-1}k_1)b \tag{A.4}$$

$$\delta = (\gamma_X + k_1 b)(\gamma_Y + k_{-1} + k_2 b)(\gamma_Z + k_{-2}) - (\gamma_X + k_1 b)k_{-2}k_2 b - (\gamma_Z + k_{-2})k_{-1}k_1 b \tag{A.5}$$

The set of decay constants, λ_1, λ_2 and λ_3 obtained by standard methods was calculated for various physically meaningful situations with unimolecular and diffusion controlled pseudo-unimolecular steps. Species' natural decay rate constants, $\gamma_X = 1/\tau_{f,X}$, $\gamma_Y = 1/\tau_{f,Y}$ and $\gamma_Z = 1/\tau_{f,Z}$, in the range of those extracted from the fluorescence decays are used in the calculations. In Table A.1, the results are

Table A.1
Results of three-state excited state kinetic modelling of Scheme 2

b (μM)	τ_X ($\times10^{-9}$ s)	τ_Y ($\times10^{-9}$ s)	τ_Z ($\times10^{-9}$ s)	k_1 ($\times10^9$ M^{-1} s^{-1})	k_{-1} ($\times10^9$ s^{-1})	k_2 ($\times10^9$ M^{-1} s^{-1})	k_{-2} ($\times10^9$ s^{-1})	$-1/\lambda_1$ ($\times10^{-9}$ s)	$-1/\lambda_2$ ($\times10^{-9}$ s)	$-1/\lambda_3$ ($\times10^{-9}$ s)
0	1.4	1.4	1.4	0	0	0	0	1.4	–	–
900[a]	1.4	0.6	3.3	6.73	1	6.73	1	0.372	0.446	0.643
900[a]	1.4	0.6	3.3	6.73	0.1	6.73	1	0.784	1.100	1.475
900[a]	1.4	0.6	3.3	6.73	1	6.73	0.1	0.385	0.497	0.864
900[a]	1.4	0.6	3.3	6.73	0.1	6.73	0.1	0.567	0.695	1.062
900[a]	1.4	0.6	3.3	6.73	0.01	6.73	0.01	0.590	0.722	1.111
900[a]	1.4	0.6	3.3	6.73	0	6.73	0	0.593	0.725	1.117

[a] The results for $b = 90$, 3100 and 9000 μM differ from the ones for $b = 900$ μM in the last decimal places only.

shown. It is clear from comparisons among data therein that short components should dominate the decay kinetics if β-cyclodextrin detachment occurs extensively. The association contribution is expected to be small for the experimental β-cyclodextrin concentrations in the time scale of rhodamine's singlet-excited states.

References

[1] J. Szejtli, Chem. Rev. 98 (1998) 1743–1753.
[2] K. Uekama, F. Hirayama, T. Irie, Chem. Rev. 98 (1998) 2045–2076.
[3] A. Douhal, Chem. Rev. 104 (2004) 1955–1976.
[4] M.V. Rekharsky, R.N. Goldberg, F.P. Schwarz, Y.B. Tewari, P.D. Ross, Y. Yamashoji, Y. Inoue, J. Am. Chem. Soc. 117 (1995) 8830–8840.
[5] R.P. Haugland, Handbook of Fluorescent Probes and Research Chemicals, Molecular Probes Inc., Eugene, 1996.
[6] M. Ogata, O. Inanami, M. Nakajima, T. Nakajima, W. Hiraoka, M. Kuwabara, Photochem. Photobiol. 78 (2003) 241–247.
[7] Y. Liu, Y. Chen, S.X. Liu, X.D. Guan, T. Wada, Y. Inoue, Org. Lett. 3 (2001) 1657–1660.
[8] G.M.M. Medeiros, M.F. Leitão, S.M.B. Costa, J. Photochem. Photobiol. A: Chem. 72 (1993) 225–233.
[9] J. Olmsted III, J. Phys. Chem. 83 (1979) 2581–2584.
[10] J.A.B. Ferreira, S.M.B. Costa, L.F. Vieira Ferreira, J. Phys. Chem. A 104 (2000) 11909–11917.
[11] N.V. Dubinin, L.M. Blinov, S.V. Yablonskii, Opt. Spectrosc. 44 (1978) 473–475.
[12] D.V. O' Connor, D. Philips, Time-correlated Single Photon Counting, Academic Press, New York, 1984.
[13] K. Levenberg, Quart. Appl. Math. 2 (1944) 164–168.
[14] D. Marquardt, SIAM J. Appl. Math. 11 (1963) 431–441.
[15] P. Debye, Polar Molecules, Dover, New York, 1929.
[16] L. Onsager, J. Am. Chem. Soc. 58 (1936) 1486–1493.
[17] N. Mataga, T. Kubota, Molecular Interactions and Electronic Spectra, Marcel Dekker, New York, 1970.
[18] C.J.F. Böttcher, Theory of Electric Polarisation, Elsevier, Amsterdam, 1973.
[19] J.A.B. Ferreira, S.M.B. Costa, J. Mol. Struct. 565–566 (2001) 35–38.
[20] J.A.B. Ferreira, S.M.B. Costa, Chem. Phys. 273 (2001) 39–49.
[21] B.S. Brunschwig, S. Ehrenson, N. Sutin, J. Phys. Chem. 91 (1987) 4714–4723.
[22] R.L. Schiller, S.F. Lincoln, J.H. Coates, J. Chem. Soc., Faraday Trans. I 83 (1987) 3237–3248.
[23] S. Vajda, R. Jimenez, S.J. Rosenthal, V. Fidler, G.R. Fleming, E.W. Castner Jr., J. Chem. Soc., Faraday Trans. 91 (1995) 867–873.
[24] J.A.B. Ferreira, S.M.B. Costa, J. Chem. Phys. 120 (2004) 8095–8106.
[25] S.J. Strickler, R.A. Berg, J. Chem. Phys. 37 (1962) 814–820.
[26] J. Widengren, U. Mets, R. Rigler, J. Phys. Chem. 99 (1995) 13368–13379.
[27] R.F. Grote, J.T. Hynes, J. Chem. Phys. 73 (1980) 2715–2732.